Cellulose (2005) 12:339–349
DOI 10.1007/s10570-005-2200-5

Structural micro-heterogeneities of crystalline Iβ-cellulose

Karim Mazeau
Centre de Recherches sur les Macromolècules Végétales (CERMAV–CNRS), Affiliated with the Joseph Fourier University, ICMG FR 260.7 BP 53, 38041 – Grenoble Cedex 9 – France
(e-mail: karim.mazeau@cermav.cnrs.fr)

Received 26 August 2004; accepted in revised form 14 February 2005

Key words: Cellulose, Conformational analysis, Crystalline structure, Iβ-allomorph, Molecular dynamics, Molecular modelling, Native phase

Abstract

The crystal structure of the native Iβ-allomorph of cellulose [Nishiyama et al. 2002. *J. Am. Chem. Soc.* 124: 9074–9082] reveals subtle but significant conformational differences between the two different chains and also a multiplicity of positions of the hydrogen atoms of the HO_2 and HO_6 hydroxyl groups. Two structures differing in the hydrogen bonding networks were then proposed, however, the static or dynamic origin of the observed disorder remains to be specified. Molecular modelling was used to address this question: 18 minicrystal and 2 macrocrystal models of cellulose were generated differing by the initial orientations of the HO_2 and HO_6 hydroxyl groups; among which the two proposed structures (called N1 and N16) together with a random structure which respect the experimental percentage of hydroxyl hydrogen orientations. Results showed that only 10 of the studied combinations were stable, the major structure (N1) defined by crystallographers was estimated viable whereas not the minor one (N16). All the calculated data from the retained crystals, which describe the solid dimensions, the individual chain conformations and the supermolecular organisation, 1/ remained stable at their equilibrium value during the dynamics and 2/ were sensitive to the initial positions of the hydrogen atoms. Analysis of the hydrogen bonds revealed that sheet stacking might be stabilised by unexpected hydrogen bonds in addition to hydrophobic interactions. Our results thus favoured local disorders which involve a limited number of chains; they revealed the structural microheterogeneity of the Iβ-phase of cellulose and a complex disorder of its corresponding hydrogen bonding networks.

Introduction

The crystal structures of the two Iα- and Iβ-allomorphs of native cellulose have been recently reported (Nishiyama et al. 2002, 2003; Jarvis 2003). Although their gross general structural characteristics were established for a long time, unexpected features are highlighted. Actually, the two independent chains of the Iβ-allomorph are conformationally different; values experienced by the glycosidic bond torsion angles differ, from one chain to the other, by 10° and 5° for the Φ and Ψ angles, respectively (see Figure 1 for the definition of the atom labelling and torsion angles definition). Similarly, ω torsion angles that describe hydroxymethyl group position differ by 12°.

Importantly, the experimental data is interpreted by a conformational disorder of the positions of the hydroxyl hydrogen atoms. Two radically different positions for each of the HO_2

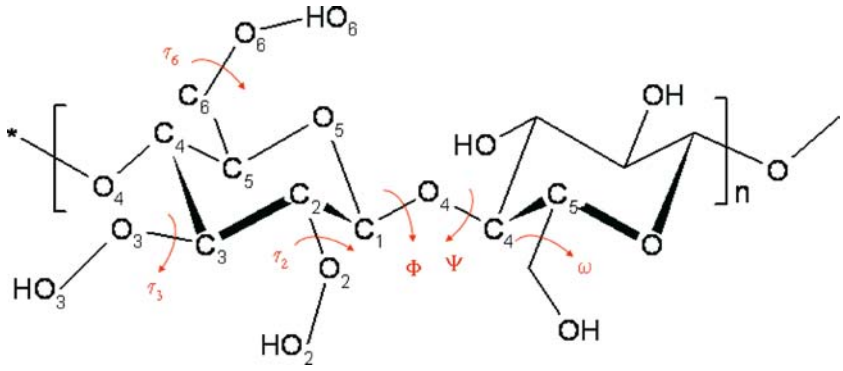

Figure 1. Schematic representation of the cellulose chain, atom labelling and torsion angles definitions. Φ: O_5–C_1–O_4–C_4; Ψ: C_1–O_4–C_4–C_5; ω: O_5–C_5–C_6–O_6; τ_2: C_3–C_2–O_2–HO_2; τ_3: C_4–C_3–O_3–HO_3; τ_6: C_5–C_6–O_6–HO_6. For clarity, aliphatic hydrogen atoms are omitted.

and HO_6 hydroxyl groups could exist; consequently, each of the τ_2 and τ_6 torsion angles adopts two different values. The experimental data are then logically interpreted by two structures differently populated, each being stabilised by a distinct hydrogen bonding network, as shown in Figure 2.

The Iβ-allomorph of cellulose has not yet revealed all its structural details, an important question emerged from the experimental study: is the positional disorder observed for the HO_2 and HO_6, which depend the hydrogen bonding networks, static or dynamic? Crystallographic methods give only a static view of the studied solid; dynamics and/or conformational disorder might be revealed by the temperature factors; unfortunately this information is rarely used. Different assumptions were then expressed: 1/ the two hydrogen bonding networks could cohabit within the same crystal, at different locations. 2/ the two hydrogen bonding networks could be in dynamic equilibrium; then they are found everywhere in the crystal and fast exchange occur. Finally 3/ the situation could be far more complex and many intermediate structures between the two limit organisations could coexist.

Molecular modelling has often been used to study the native forms of crystalline cellulose; unfortunately the coordinates used to build the initial structure were both incomplete and partially erroneous, which questions the acquired results. The goal of this study is to reconsider the modelling of the Iβ-allomorph of cellulose by using the exact coordinates of the atoms as they are determined by using crystallography and to address the question of the static or dynamic nature of the disorder.

Experimental

Modelled systems

All the computational details have been described in our preceding study (Mazeau and Heux 2003), therefore only the general aspects of the procedure will be recalled here. Periodic crystal structures from the previously published coordinates (Nishiyama et al. 2002) have been generated following the protocol described in reference (Mazeau and Heux 2003): the computational boxes consist of duplicates of the primitive cell; coordinates of cellulose chains along with periodic images were generated and positioned in a crystalline super-cell subjected to periodic boundary conditions in all three directions. The edge dimensions of the super-cell is exactly the sum of all the elementary cells that were used. The space group of each crystal is P_1; this space group is lacking symmetry operations therefore all the chains within the cell are independent. Each chain possesses only four independent residues; they were however all covalently connected to their periodic images at their two ends, mimicking infinitely long chains. The generated crystal structures differed by the initial orientation of the hydrogen atoms of the HO_2 and HO_6 hydroxyl groups, as indicated in Table 1. Sixteen minicrystals (referred N1–N16) and 2 macrocrystals (R1 and R2) which consist of 32 and 128 independent glucose units, respectively were considered. The orientation of the HO_2 and HO_6 hydroxyl groups varied systematically in the 16 minicrystals (Table 1).

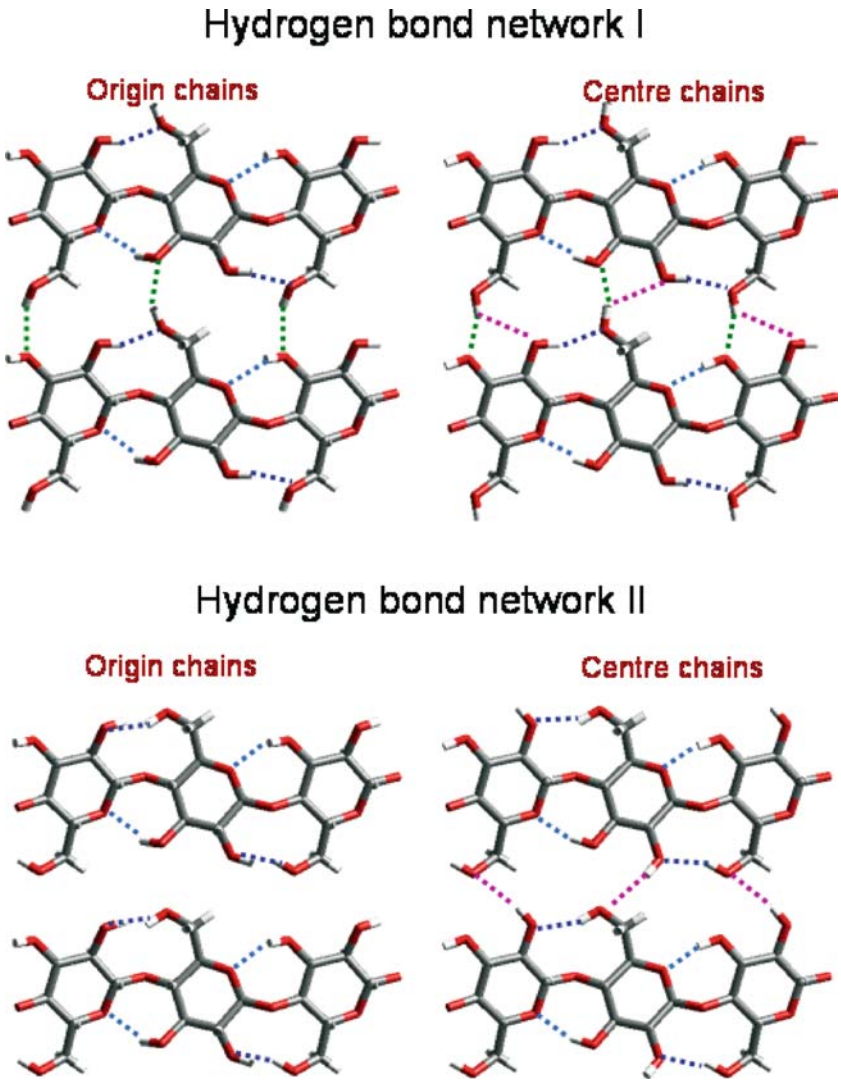

Figure 2. The two experimental hydrogen bonds networks; adapted from (Nishiyama et al. 2002).

The two hydrogen bond networks that are defined by the crystallographic study are considered in the two limit structures, N1 and N16 corresponding to the first and the second networks, respectively. In contrast, the orientation of the HO_2 and HO_6 hydroxyl groups were randomly attributed in the two larger structures; macrocrystal R1 possess 80% of the HO_2 and HO_6 orientations corresponding to the first network and 20% of the second one whereas R2 macrocrystal possess an equal amount of the two orientations.

Computational details

Energy calculations were carried out by using the second-generation force-field PCFF, specially suited for polymers and other materials (Maple et al. 1988, 1994; Maple 1994; Sun et al. 1994; Sun 1995). The PCFF force field have been parameterised and validated using condensed phase properties in addition to various *ab initio* and empirical data for molecules in isolation. Furthermore this force field has successfully modelled polysaccharides; it correctly reproduces

Table 1. τ_2 and τ_6 initial values (°) of the simulated crystal structures.

	τ_2		τ_6			τ_2		τ_6	
	Origin	Centre	Origin	Centre		Origin	Centre	Origin	Centre
N1	165.0	165.9	167.7	206.2	N9	190.4	165.9	167.7	206.2
N2	165.0	165.9	167.7	64.9	N10	190.4	165.9	167.7	64.9
N3	165.0	165.9	66.3	206.2	N11	190.4	165.9	66.3	206.2
N4	165.0	165.9	66.3	64.9	N12	190.4	165.9	66.3	64.9
N5	165.0	190.2	167.7	206.2	N13	190.4	290.2	167.7	206.2
N6	165.0	190.2	167.7	64.9	N14	190.4	290.2	167.7	64.9
N7	165.0	190.2	66.3	206.2	N15	190.4	290.2	66.3	206.2
N8	165.0	190.2	66.3	64.9	N16	190.4	290.2	66.3	64.9
R1	165.0	165.9	167.7	206.2	R2	165.0	165.9	167.7	206.2
	(80%)	(80%)	(80%)	(80%)		(50%)	(50%)	(50%)	(50%)
	190.4	190.2	66.3	64.9		190.4	190.2	66.3	64.9
	(20%)	(20%)	(20%)	(20%)		(50%)	(50%)	(50%)	(50%)

structures and properties of amorphous and crystalline solids of cellulose (Mazeau and Heux 2003) together with the cellulose surface interactions with aromatic species (Mazeau and Vergelati 2002; Da Silva Perez et al. 2004). For the Coulombic term, the dielectric constant value was set to 1. All atoms are treated explicitly.

Each simulated crystal was subjected to energy minimisation before the actual molecular dynamics simulation was started. The simulations were carried out for 1 ns each after another 100 ps equilibration time.

The standard Verlet (Verlet 1967) algorithm was used to integrate Newton's law of motion with a time step of 0.001 ps. For the canonical N,P,T dynamics (Parrinello and Rahman 1981), the relaxation time constant and the mass-like parameter which determines the rate of change of volume/shape matrix were set to 0.1 ps and 1.00, respectively. Each molecular dynamics run was started by assigning initial velocity for the atoms according to a Boltzmann distribution at $2*T$, T being the target temperature. The velocities of the atoms were quickly scaled down so that the final temperature of atoms was T. The total external pressure was maintained at 1 atm., and Nosé's algorithm (Nosé 1984) was used to keep the cell temperature constant at 300 K in the molecular dynamics simulation.

All calculations were performed at the Centre d'Expérimentation et de Calcul Intensif, CECIC, Grenoble.

Results and discussion

Energetics

Average potential energies of the modelled crystal structures are reported in Figure 3. Two groups of eight structures each can be easily identified for the (N1–N16) minicrystals; high energy structures are not stable and are consequently rejected. In contrast, the remaining eight low energy structures are favourable, their average energy is −17 kcal/mol/disaccharide in good agreement with our previous modelling (Mazeau and Heux 2003) (−12 kcal/mol/disaccharide for the Iα-phase and −14 kcal/mol/disaccharide for the Iβ-allomorph). The present estimated energy is lower than those reported in our previous simulation, probably because the initial coordinates that were used to

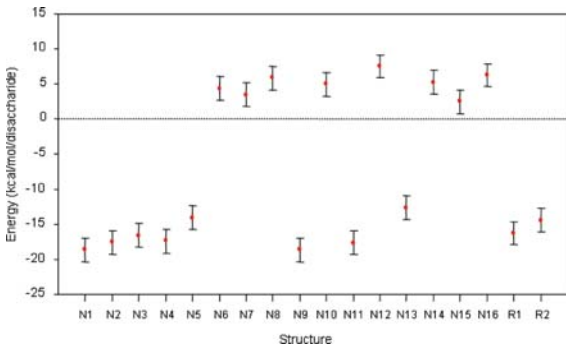

Figure 3. Energies (kcal/mol/disaccharide) of the simulated crystals.

build the different crystals were more reliable. Stability of the N1 structure suggests that our modelling is in agreement with the crystallographic analysis on the major form. However, the instability of the N16 structure shows that the experimentally defined minor form might be a virtual structure, without real physical meaning. Moreover the many stable 'intermediate' structures strongly suggests that the positional disorder of the hydrogen atoms of the O_2 and O_6 hydroxyl groups could be statistically distributed within the crystal. Equilibrium energies of the random (R1–R2) macrocrystals are in the range of those estimated for the minicrystals.

Predicted densities and cell parameters

Equilibrium densities together with the equilibrium edge lengths of the primitive cells of the 10 selected structures are reported in Table 2. Predicted densities are in the range 1.45–1.59 g/cm^3. No individual structure exactly reproduce the target density of 1.636 g/cm^3 estimated from the experimental primitive crystal cell dimensions, predicted values are systematically lower than the expected one. The average estimated density of 1.513 g/cm^3 differs from the experimental one by less than 8%.

Already suggested by the lower densities of the models, cell dimensions *a*, *b* and *c* are almost systematically larger than the experimental values. Average values of 7.90 ± 0.35 Å, 8.54 ± 0.31 Å and 10.70 ± 0.09 Å for *a*, *b* and *c*, respectively correspond to deviations with respect to the experimental data of 1.5, 4 and 3%, respectively. Cellulose chains are predicted too extended than expected; this probably results from defaults of the force field parameters but it is not expected to have more than a minor influence on the results of the simulations. Values found for *c* are in the range to those reported in other modelling studies. A maximal deviation of 2% is reported in our preceding study which uses the same force field; other force fields do not give better results: deviations in the range 0.8 to 5% are obtained by NPT molecular dynamics (Ganster and Blackwell 1996; Kroon-Batenburg et al. 1996; Neyertz et al. 2000) while the average deviation of 7% is predicted for a non-periodic crystal (Baird et al. 1998). However, to explore the concept of structural microheterogeneities, only the extent of variations of a parameter from one structure to another is relevant. In this spirit, experimental data supports our conclusions as unit cell dimensions of native celluloses are reported to be dependant on the origin of the sample, by 1 and 0.6% for *a* and *b*, respectively (Ioelovich and Larina 1999) and by 0.7% for *c* (Davidson et al. 2004). Furthermore, analysis of crystalline structures of molecular fragments analogous of cellulose demonstrate that the advance of residue along the chain axis between 5.04 and 5.27 Å is influenced by packing forces (French and Johnson 2004).

The average cell angles are $89.96 \pm 0.15°$, $90.06 \pm 0.20°$, $94.18 \pm 4.4°$ for α, β and γ, respectively. The α and β angle are constant from one structure to the other, they correctly reproduce the experimental values. Note that these two parameters are experimentally exactly at 90° because of the monoclinic space group. No symmetry operation is imposed in our calculations and these two cell

Table 2. Energies (kcal/mol/disaccharide), densities (g/cm^3) and cell parameters (lengths in Å; angles in °) of the modelled (Ni and Ri) and experimental structures (X).

	Energy	Density	*a*	*b*	*c*	α	β	γ
N1	−18.63	1.45	8.11	8.56	10.72	90.00	89.99	95.32
N2	−17.59	1.50	7.81	8.51	10.78	90.00	90.00	92.08
N3	−16.57	1.54	7.70	8.50	10.69	89.86	89.97	89.31
N4	−17.34	1.49	7.91	8.53	10.74	89.67	89.90	93.73
N5	−14.09	1.54	7.71	8.70	10.67	90.00	90.00	102.13
N9	−18.60	1.45	8.11	8.56	10.72	90.00	90.00	95.31
N11	−17.64	1.52	7.98	8.24	10.79	90.23	89.91	87.19
N13	−12.64	1.49	7.95	8.77	10.57	90.00	90.00	100.67
R1	−16.25	1.56	7.67	8.51	10.60	89.78	90.26	94.33
R2	−14.38	1.59	6.82	9.48	10.48	90.03	90.60	91.74
X		1.64	7.78	8.20	10.38	90.00	90.00	96.55

angles are free to evolve during the dynamics. Therefore small differences from the ideal value of 90° are not surprising. The cell angle γ shows the largest variations; from 87° to 102°.

The largest standard deviation of the cell parameters concerns the a dimension while dimension c that corresponds to the fibre axis is remarkably constant; this difference can be related to the thermal expansion of crystalline cellulose, which is observed anisotropic (Wada 2002).

Structural parameters

Calculated data are analysed from 32 independent units distributed in 4 layers of cellulose chains for the minicrystals and from 128 residues distributed in 8 layers for the macrocrystals. Distinction is made between origin and centre layers.

In this section, we are interested by the torsion angles that describe the conformations of the individual chains. Atom numbering and definition of the torsion angles are indicated in Figure 1. Torsion angles around the glycosidic bonds (Φ and Ψ) together with torsion angles that describe the orientations of the hydroxymethyl groups (ω) and the different hydroxyl groups (τ_2, τ_3 and τ_6) displayed an identical conformational behaviour. In each structure, those conformational parameters converged as early as the end of the minimisation process to their equilibrium geometries which were conserved throughout the trajectory; no conformational transition from one stable conformation to another one is observed. Furthermore systematic conformational differences between 'origin' and 'centre' sheets are observed, as average equilibrium values of the torsion angles differ from one structure to the other and also from one sheet to the other within a structure.

The correlation between Φ and Ψ is reported in Figure 4. All values explored by Φ and Ψ are located within the main low energy area of the corresponding disaccharide (French and Dowd 1993). Absolute predicted values of both torsion angles differ from the ones deduced from the experimental study. In particular, they are more homogeneous and Φ values are systematically lower than the experimental ones whereas Ψ values are higher. Interestingly, values deviates slightly from the exact the iso-$n = 2$ helical contour, displayed as a dashed line in Figure 4.

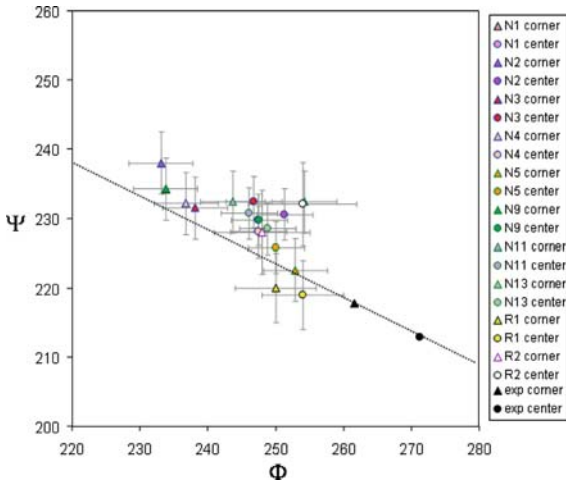

Figure 4. Correlation between Φ and Ψ torsion angles; the dashed line corresponds to the iso-$n = 2$ helical parameter.

All hydroxymethyl groups explore the tg orientation; values adopted by ω torsion angles range between 150° and 188° (Figure 5). Experimentally, this torsion angle differ by 33°, the origin chains explore a lower value than the centre chains. Our calculations also reproduce differences from one sheet to the other in the values adopted by this angle from 5° to 38°. In contrast, the origin chains adopt larger values than the centre chains.

Values experienced by the torsion angles τ that describes the orientations of the hydroxyl groups are given in Figure 6. Most of HO_3 groups adopt orientations comparable to the ones observed in crystallography. In contrast, the orientations of the HO_2 and HO_6 hydroxyl groups converge to

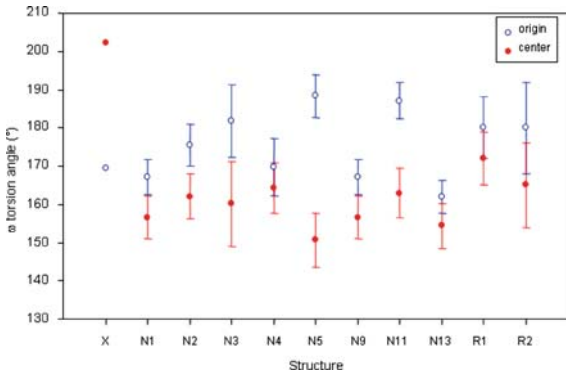

Figure 5. Hydroxymethyl group orientations of the crystalline structure (X) and the different modelled ones: ω torsion angle (°).

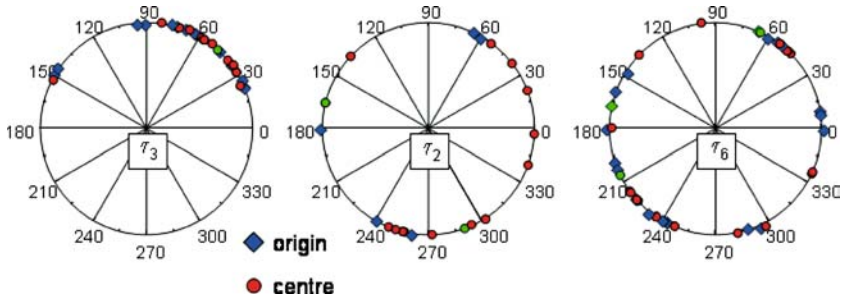

Figure 6. Orientation (°) of the different hydroxyl groups O_3, O_2 and O_6. Symbols filled in green indicate values observed in the reference crystal structure.

both the observed values of the torsion angles τ_2 and τ_6 and also to atypical angular domains.

Supramolecular organisation

In this section, the molecular and supermolecular organisations are analysed; this means the global conformation of the individual chains, pictured by their global extension together with the position of a given chain relative to the others. To access these properties, the radial distribution functions specifically calculated for the glycosidic oxygens O_4 are used. O_4-RDFs are calculated for a maximal distance of 9 Å. Figure 7 gives a superposition of three O_4-RDF profiles of the structure N1: the profile calculated by considering all the O_4 oxygen atoms (called hereafter totalRDF) and those profiles which separately considers the O_4 atoms of each sheet (called originRDF and centreRDF).

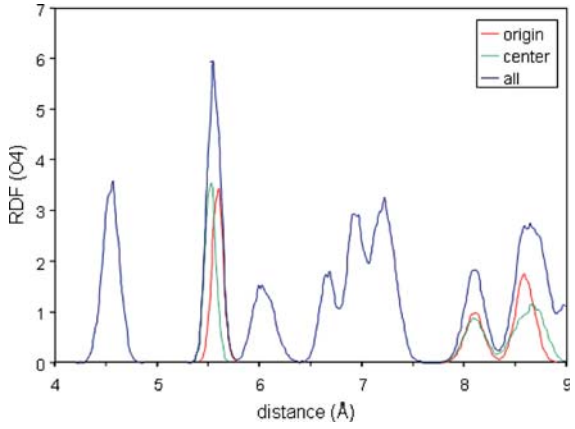

Figure 7. Profiles of the radial distribution functions calculated considering only the O_4 oxygen atoms.

Only three peaks appear on the two individual centreRDF and originRDF profiles; two of them are particularly informative. The peak located at about 5.6 Å corresponds to the distance between two consecutive O_4 in a chain, its exact position in the RDF profiles give a measure on the fluctuation of helical extension of the individual chains. The peak at 8.6 Å corresponds to the distance between O_4 of two neighbour chains within a sheet; its position is a signature of the 'inplane' ultrastructural organisation. Many supplementary peaks appear when one considers all O_4 atoms in the totalRDF profile; the forest of peaks, located at 6.5 to 7.5 Å, for example, is useless for our goal as peaks cannot be individualised. Peak at 4.6 Å corresponds to a distance between O_4 atoms of different chains which belong to two consecutive sheets; its location indicates therefore the 'out of plane' supermolecular organisation of the chains, between two sheets. Exact positions of those three peaks for each structure are reported in Table 3. The reported characteristic distances systematically differ from the centre chains to the corner ones in each structure and also differ from one structure to the other. Such result shows that the cellulose chains significantly slide the ones with respect to the other in and between the sheets. Structural microheterogeneity is therefore not limited to the conformation of the individual chains; it concerns also the organisation of the chains in the crystal.

Hydrogen bonds

The numerous hydroxyl groups and acetal oxygens that bear each cellulose chain favour the creation

Table 3. Position of the three relevant peaks (Å) in the RDFs profiles.

	Peak									
	5.6				8.6				4.4	
	Origin1	Origin2	Center1	Center2	Origin1	Origin2	Center1	Center2		
N1	5.53	5.53	5.61	5.61	8.55	8.55	8.55	8.57	4.57	
N2	5.63	5.63	5.55	5.53	8.55	8.51	8.51	8.53	4.71	
N3	5.55	5.53	5.55	5.55	8.39	8.41	8.51	8.51	4.63	
N4	5.53	5.51	5.57	5.59	8.47	8.45	8.51	8.55	4.59	
N5	5.55	5.53	5.49	5.51	8.73	8.71	8.71	8.67	4.41	
N9	5.51	5.51	5.59	5.59	8.59	8.57	8.57	8.57	4.55	
N11	5.63	5.61	5.61	5.65	8.23	8.25	8.29	8.17	4.71	
N13	5.59	5.61	5.53	5.53	8.75	8.77	8.77	8.77	4.33	
R1	5.55		5.52		8.60		8.30		4.45	
R2	5.45		5.50		8.52		8.13		4.62	
					8.21		8.21			
X	5.49		5.43						4.41	
					8.71		8.69			

of hydrogen bonds, which strongly contribute to stabilise the auto-associations of the chains. The two hydrogen bond networks observed experimentally are given in Figure 2 and Table 4. Table 4 also gives the hydrogen bond statistics of each modelled microstructure.

The method traditionally used to detect a hydrogen bond is geometric: two oxygen atoms are considered hydrogen bonded if the distance between the hydrogen of the donor and the oxygen acceptor is lower than 2.5 Å and if the angle between the oxygen donor, the hydrogen donor and the oxygen acceptor larger than 90°. Note that such criteria are more restrictive than those used in the crystallographic study. Results show that the predicted hydrogen bond networks strongly depend on the structure and hence of the initial position of the hydrogen atoms of the hydroxyl groups. However, statistically the ensemble of considered structures shows the following strong similarity with the experimental data: in the reference crystal structure, the helical conformations of the chains are stabilised by two systematic intramolecular hydrogen bonds: $O_3 \cdots O_5$, (O_3

Table 4. Observed (Net) and predicted hydrogen bonds (statistics expressed in %).

	Intramolecular			Intermolecular							
				Intrasheet				Intersheet			
Donor	O3	O2	O6	O6	O3	O6	O2	O6	O2	O6	O2
Acceptor	O5	O6	O2	O3	O6	O2	O6	O4,O5	O2	O2	O3
Net1 origin	X	X		X		X					
Net1 centre	X	X		X							
Net2 origin	X		X								
Net2 centre	X		X				X				
N1	84	85	0	100	0			6			
N2	33	52	50	50	50						
N3	69	51	22	42	0			35	61	39	
N4	81	46	13	77	0			42	75		
N5	81	50	0	82	0						68
N9	85	84	0	99	0			7			
N11	69	80	9	50	19						
N13	93	40	0	50	0			8			75
< model >	74	61	12	69	9	0	0	12	17	5	18

donor) and $O_2\cdots O_6$; (O_2 donor in the first network and O_6 donor in the second network) the later also stabilise the tg orientation of the hydroxymethyl groups. Our results show that the $O_3\cdots O_5$ (O_3 donor) hydrogen bond is extremely persistent; it represents more than 75% of the total simulation time. Similarly, the $O_2\cdots O_6$ hydrogen bond persists at 73% of the total simulated duration, the O_2 oxygen is much more donor (61%) than the O_6 atom (12%). Such hydrogen bonds are not represented at 100% because on the one hand, the geometric criteria used might be too restrictive. On the other hand, such intramolecular hydrogen bonds are in competition with intermolecular ones, in structures N1 and N9, a bifurcated hydrogen bond is observed $O_2\cdots O_6$ evidently and also $O_6\cdots O_4$ or $O_6\cdots O_5$ the acetal oxygen atoms belong to chains of the next sheet (see Figure 8) this event is however rare. Moreover, centre chains of structures N5 and N13 do not form such $O_2\cdots O_6$ hydrogen bonds, in both cases, HO_2 hydroxyl group is engaged in intermolecular hydrogen bonds.

Intermolecular hydrogen bonds are also experimentally observed, occurring only between the chains of the same sheet. Such hydrogen bonds stabilise the intrasheet crystal structure cohesion. Two such hydrogen bonds are experimentally observed: $O_6\cdots O_3$ (O_6 donor) concerns only the chains of the first network while it is absent in the second one. $O_6\cdots O_2$ also occurs to a minor extent, it concerns only the centre chains of both networks (O_6 donor in the first network whereas O_2 donor in the second network). Statistically the hydrogen bond between O_3 and O_6 is observed for more than 78% of the simulated time. The O_6 hydroxyl group act mainly as the donor (69%) whereas the O_3 is rarely the donor (9%). In some structures, for example N1 (Figure 6), this hydrogen bond is systematic (100%), in other structures the $O_3\cdots O_6$, O_3 donor or acceptor are in competition, such as the centre chains of N2 and finally structures such as N3 (origin chains) or N9 for which this hydrogen bonds is not observed at all.

Importantly, the ensemble of considered structures shows also interesting divergences with the experimental data. On the one hand, no intrasheet $O_2\cdots O_6$ hydrogen bond could be detected; this is not surprising since this hydrogen bond is experimentally reported as geometrically out of our limit. The interaction between these two groups is thus very weak and consequently contribute only a little to the stabilisation of the supermolecular organisation. Cellulose chain sliding during dynamics increases the distance between O_2 and O_6 atoms of neighbour chains thus further minimising the influence of this hydrogen bond. Figure 9 gives two examples of calculated intrasheet hydrogen bonds. In the structure N1, the $O_2\cdots O_6$ average oxygen acceptor to hydrogen donor distance is 3.5 Å and the average angle is 75°, this geometry is not compatible with a significant hydrogen bond.

In addition to these 'classical' hydrogen bonds, a significant amount of intermolecular and intersheets hydrogen bonds are detectable. They significantly contribute to intersheet crystal stabilisation as they are observed persistent in structures N3, N4, N5 and N13. For the other four minicrystals, only structures N2 and N11 have no such intersheet hydrogen bonds while such intersheet hydrogen bonds appear occasionally and disappear rapidly in structures N1 and N9. However, on average the statistical significance of such hydrogen bonds is minor; it represents no more than 18% of the total simulated time (Table 4).

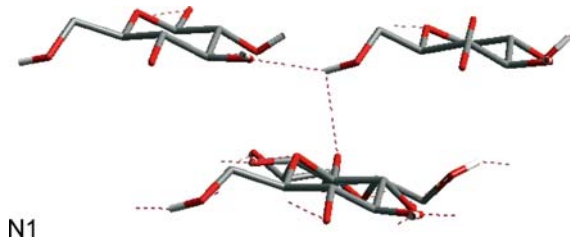

Figure 8. The bifurcated intermolecular hydrogen bonds: intrasheet $O_6\cdots O_3$ and intersheet $O_6\cdots O_4$.

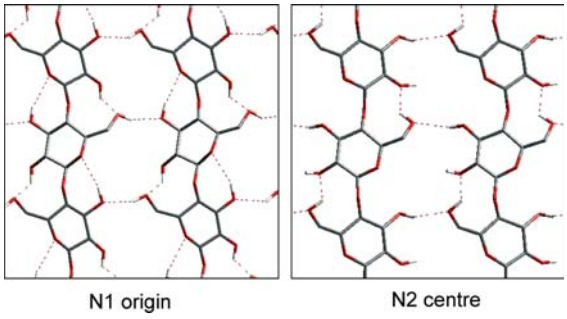

Figure 9. Two representative examples of intramolecular and 'in plane' intermolecular hydrogen bonds.

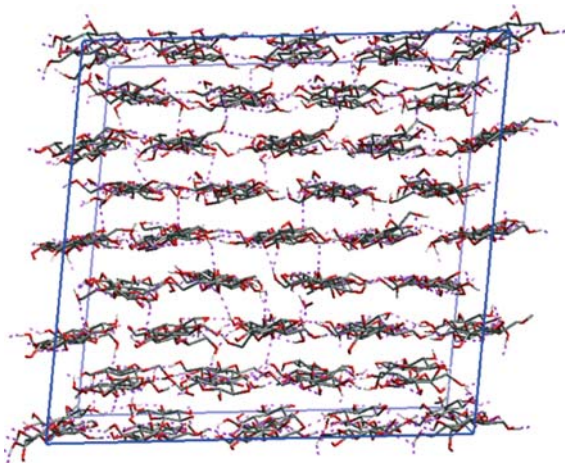

Figure 10. Hydrogen bonds in the R1 structure.

Figure 10 gives a snapshot of the R1 macrocrystal extracted from the dynamic trajectory which shows all the computed unusual intersheets hydrogen bonds.

Conclusions

Modelling the Iβ-allomorph of cellulose has been reconsidered in the light of the recent experimental diffraction studies (Nishiyama et al. 2002). We have simulated by molecular dynamics eight minicrystal and two macrocrystal structures, differing by the initial orientation of the HO_2 and HO_6 hydroxyl groups. No conformational interconversion from one minimum to another is observed and all the predicted equilibrium structural characteristics are sensible to the initial position of the hydrogen atoms of the hydroxyl groups. The experimentally observed conformational differences between the different chains appear by molecular modelling as well, predicted values of the Φ, Ψ and ω torsion angles are however more homogeneous than those observed. In contrast, torsion angles that define the HO_2 and HO_6 conformations adopt a wide range of values; such modelled disorder is larger than the observed one. As a consequence, the hydrogen bond networks are calculated much more complicated than the two observed ones. In addition to the 'classical' hydrogen bonds several possibilities of intersheet hydrogen bonds have been evidenced. Molecular modelling clearly shows geometrical variability in the Iβ-allomorph of crystalline cellulose, corresponding to stable structural microheterogeneities.

References

Baird M.S., O'Sullivan A.C. and Banks W.B. 1998. A native cellulose microfibril model. Cellulose (London) 5: 89–111.

Da Silva Perez D., Ruggiero R., Morais L.C., Machado A.E.H. and Mazeau K. 2004. Theoretical and experimental studies on the adsorption of aromatic compounds onto cellulose. Langmuir 20: 3151–3158.

Davidson T.C., Newman R.H. and Ryan M.J. 2004. Variations in the fibre repeat between samples of cellulose I from different sources. Carbohydrate Res. 339: 2889–2893.

French A.D. and Dowd M.K. 1993. Conformational analysis of cellobiose with MM3. Cellulose: Chem. Biochem. Mater. Aspects, Horwood, London, UK CODEN: 59RAA9, pp. 51–56.

French A.D. and Johnson G.P. 2004. What crystals of small analogs are trying to tell us about cellulose structure. Cellulose (Dordrecht, Netherlands) 11: 5–22.

Ganster J. and Blackwell J. 1996. NpH-MD-simulations of the elastic moduli of cellulose II at room temperature. J. Mol. Model. [Electronic Publication] 2: 278–285.

Ioelovich M. and Larina E. 1999. Parameters of crystalline structure and their influence on the reactivity of cellulose I. Cellulose Chem. Technol. 33: 3–12.

Jarvis M. 2003. Chemistry: cellulose stacks up. Nature (London, United Kingdom) 426: 611–612.

Kroon-Batenburg L.M.K., Bouma B. and Kroon J. 1996. Stability of cellulose structures studied by MD simulations? Could mercerized cellulose II be parallel. Macromolecules 29: 5695–5699.

Maple J.R. 1994. Derivation of class II force fields. 3. Characterization of a quantum force field for the alkanes. Israel J. Chem. 34: 195–231.

Maple J., Dinur U. and Hagler A.T. 1988. Derivation of force fields for molecular mechanics and dynamics from *ab initio* energy surfaces. Proc. Natl. Acad. Sci. USA 85: 5350–5354.

Maple J.R., Hwang M.J., Stockfisch T.P., Dinur U., Waldman M., Ewing C.S. and Hagler A.T. 1994. Derivation of class II force fields. I. Methodology and quantum force field for the alkyl functional group and alkane molecules. J. Comp. Chem. 15: 162–182.

Mazeau K. and Heux L. 2003. Molecular dynamics simulations of bulk native crystalline and amorphous structures of cellulose. J. Phys. Chem. B 107: 2394–2403.

Mazeau K. and Vergelati C. 2002. Atomistic modeling of the adsorption of benzophenone onto cellulosic surfaces. Langmuir 18: 1919–1927.

Neyertz S., Pizzi A., Merlin A., Maigret B., Brown D. and Deglise X. 2000. A new all-atom force field for crystalline cellulose I. J. Appl. Polymer Sci. 78: 1939–1946.

Nishiyama Y., Langan P. and Chanzy H. 2002. Crystal structure and hydrogen-bonding system in cellulose Ib from synchrotron X-ray and neutron fiber diffraction. J. Am. Chem. Soc. 124: 9074–9082.

Nishiyama Y., Sugiyama J., Chanzy H. and Langan P. 2003. Crystal structure and hydrogen bonding system in cellulose Ia from synchrotron X-ray and neutron fiber diffraction. J. Am. Chem. Soc. 125: 14300–14306.

Nosé S. 1984. A molecular dynamics method for simulations in the canonical ensemble. Mol. Phys. 52: 255–268.

Parrinello M. and Rahman A. 1981. Polymorphic transitions in single crystals: a new molecular dynamics method. J. Appl. Phys. 52: 7182–7190.

Sun H. 1995. *Ab initio* calculations and force field development for computer simulation of polysilanes. Macromolecules 28: 701–712.

Sun H., Mumby S.J., Maple J.R. and Hagler A.T. 1994. An *ab initio* CFF93 all-atom force field for polycarbonates. J. Am. Chem. Soc. 116: 2978–2987.

Verlet L. 1967. Computer experiments on classical fluids. I. Thermodynamical properties of Lennard–Jones molecules. Phys. Rev. 159: 98–103.

Wada M. 2002. Lateral thermal expansion of cellulose Ib and IIII polymorphs. J. Polymer Sci. Part B: Polymer Phys. 40: 1095–1102.